Research on Engineering Structures & Materials
www.jresm.org
Research Group

*Research Article*

# Experimental investigation and numerical optimization of sheet metal forming limits during deep drawing process of DD14 steel

Faouzi Hamza[*1,a], Ouzine Boussaid[2,b], Hamid Hamadache[3,c], Abdelmoumene Guedri[4,d]

[1]*Department of Mechanical Engineering, Badji Mokhtar University, Annaba, Algeria*
[2]*Department of Mechanical Engineering, Badji Mokhtar University, Research Laboratory of Research on Industrial Risks, Control and Safety, Annaba, Algeria*
[3]*Department of Mechanical Engineering, Badji Mokhtar University, Research Laboratory of Advanced Technology in Mechanical Production (LRATPM), Annaba, Algeria*
[4]*Department of Mechanical Engineering, Med Chérif Messaadia University, Souk Ahras, Algeria*

**Article Info**

*Article history:*

Received 09 Dec 2023
Accepted 26 Feb 2024

*Keywords:*

*DD14 steel;*
*Experimental investigation;*
*Numerical optimization;*
*Forming limit curve;*
*Deep drawing*

**Abstract**

This work aims to experimentally study the deep drawability of DD14 hot-rolled steel sheets and to optimize numerically the material formability. The material anisotropy was confirmed by metallographic analysis of the material and tensile tests on specimens taken in three orientations with respect to the sheet rolling direction. Where the stress-strain curves show a sensitivity of material to the Piobert-Lüders phenomenon. The die pressure and the blank holder were considered as controlling factors on plastic instability and the success of the deep drawing operation. The forming limit curves (FLC) were plotted to highlight the different deformation modes that the sheet metal underwent during the deep drawing process. The collected deep-drawn parts observation shows severe plastic instability, until fracture. The initial plastic anisotropy is determined by the Hill48 quadratic criterion and the work hardening by the Hollomon power law. It results, during the experimental tests, that the front bottom corners of the deep drawn part are the areas at high risk of damage. The various numerical simulation scenarios followed by comparisons with the experimental results, allowed us to confirm the optimum conditions that minimize the material's plastic instability risks, forming operation "Step" and BHP "Amplitude".



## 1. Introduction

The forming processes make it possible to manufacture complex mechanical parts such as vehicle body components, household appliances, kitchen utensils and many others. The deep drawing being one of these processes is characterized by the plastic deformation of a sheet in order to obtain the desired shape. To do this, a stamping operation requires three main tools: the die, the blank holder and the punch. The blank is the sheet metal to be formed, positioned and held by the blank holder pressure. The forming operation is ensured by the action of the punch, which sinks into the blank until it matches the shape of the die. This action is carried out under penetration pressure at a certain speed to give the sheet the desired geometric shape. This process, difficult to master, depends on numerous criteria linked to the geometry of the finished product, the nature of the material and the working conditions.

The plastic instability of materials is one of the main causes of necking and mechanical fracture phenomena. This phenomenon is more increased in the case of deep drawing,

[*]Corresponding author: faouzi-hamza@hotmail.fr
[a] orcid.org/0000-0002-2948-6281; [b] orcid.org/0000-0002-5655-5676; [c] orcid.org/0000-0002-3373-5738; [d] orcid.org/0000-0001-6406-8678
DOI: http://dx.doi.org/10.17515/resm2024.118me1209rs

where it results in thinning and/or wrinkling of deep-drawn metal sheets. The anisotropy and friction of the material in the deep drawing device make the problem linked to its forming more complex. Several investigations have been carried out in this area. One of the difficulties of plastic instability is the material sensitivity to the Piobert-Lüders phenomenon, which manifests in the appearance of persistent sliding bands during the elastoplastic deformation. In the presence of this phenomenon, the tensile test curves show heterogeneity of the strain and a discontinuity of the elastic limit. We then witness two values of this property, higher and lower [1]. This discontinuity of Re is more marked in mild steel and cast iron, in reason to the presence of small quantities of carbon or nitrogen [2].

It appears that the more random the distribution of carbides and more their forms are spheroidal, the more likely it is that the Piobert effect occurs. At large grain sizes, $\varepsilon_L$ becomes very small and the Lüders deformation bands disappear. However, other undesirable surface roughness makes the orange peel phenomenon appear. During sheet metal forming, differently oriented grains have the ability to deform independently, generating the formation of bands on the surface. Larger the grains more apparent the effect [3]. This phenomenon is undesirable for deep-drawing steel sheets because the deformation bands it causes are prominent on the surface after the sheets are deep-drawn [4].

The formation of the Piobert-Lüders phenomenon in ferritic mild steel has been the subject of several researches. In this context, Mazière et al. [5] studied by experimental and numerical analysis the Lüders phenomenon in low-carbon ferritic steel under simple shear load. Wenman and Chard-Tuckey [6] studied the Lüders deformation in ferritic steel tensile specimens by modeling and experimental material characterization and found some differences between the model responses when the level of plastic strain was lower than the Lüders strain presented by the material. Mao and Liao [7] studied the effects of ferrite grain size, pearlite volume fraction and pearlite interlamellar spacing on flow behavior. The study was carried out by modeling the elongation of the lüders bands and hardening behaviors of two-phase ferrite-pearlite steels under tension. Further investigations into this phenomenon have been carried out by the finite element method [8-9].

Keeler [10] introduced the forming limit diagrams. These were constructed empirically to describe the deformation states known as the Keller-Goodwin curve, these curves show combinations of major and minor strains, from which a much-localized area of thinning or necking becomes visible on the sheet metal surface. Boudeau and Gelin [11] studied the influence of macroscopic and microscopic properties on the necking of metal sheets. Doege and EI-Dsoki [12] Investigated by experimental and numerical simulation the initiation and propagation of cracks during the deep drawing process of X5 Cr Ni 18 9 steel. They were able to identify two different types of cracks which can lead to material failure. Jain et al. [13] determined experimentally the forming limit curve at necking and fracture, using a ductile fracture criterion to predict the fracture limit of aluminum sheets for automobiles.

The sensitivity of material plastic instability to the forming process parameters is also the subject of other studies. Where Kardan et al. [14] studied experimentally and by finite element method the influence of deep drawing parameters on the residual stresses evolution. Hamza et al. [15] studied by numerical simulation the deep drawing parameter's effect on the plastic strain evolution in the metal sheet during the forming operation. Habeeb et al. [16] studied how the Single-Point incremental forming process parameters impact the blank surface roughness. Rabia et al. [17] investigated how PVD coatings, lubrication conditions, and operating parameters impact tribological behavior, forming forces, and energy consumption when deep drawing is performed. An innovative test rig

will be utilized to record force-time variations, frictional interactions, and energy consumption under various conditions, such as lubrication and non-lubrication.

The blank material must be suitable for the deep drawing operation; Torkar et al. [18] determined the effect of the cementite particle/ferrite matrix interface on microcrack formation and its influence on the drawability of low-carbon steel. Some authors have proposed criteria and models as solutions to certain metal-forming problems. Ma et al. [19] proposed a ductile fracture criterion in order to predict the forming limit curve at fracture. Also, Butuc et al. [20] presented an experimental validation of a new prediction model of the forming limit curve under linear and complex deformation paths. Matin et al. [21] proposed a method for calculating the stress field corresponding to the local necking. The proposed method is designed to circumvent traditional difficulties associated with detecting and measuring strains at local necking regions of a forming limit in aluminum alloys. Stoughton and Yoon [22] determined the forming limit curve based on the stress-strain fields and discussed the parameters of the non-linear deformation. Several studies have been carried out to evaluate and analyze the formability of metal sheets. Li et al. [23] developed an analytical approach for predicting the forming limit with a non-linear strain path after pre-strained in uniaxial and biaxial tension for Aluminum alloy sheets. Kumar [24] studied the formability of different sheet materials, taking into account different parameters such as thickness, hardening coefficient and normal anisotropy. Aghaie-Khafri and Mahmudi [25] presented an analytical method to predict the forming limit curve of two aluminum alloys, with a theoretical and experimental analysis of the biaxial strain limit. Based on strains and stresses, Paul [26] contributed to the theoretical analysis of several instability criteria to construct a strain and stress-based forming limit diagrams, Including the diffuse bifurcation analysis, the neck formation of through-thickness and the shear stress-based criteria onset of through-thickness necking. Paul, in review works, explains why HER (Hole Expansion Ratio) is currently an essential topic of engineering research [27], summarizes the factors affecting FLC comprehensively to help in decision-making in material selection and process design [28] and investigate how different tensile pre-straining methods affect the high cycle fatigue, low cycle fatigue, and notch fatigue performance of automotive grade dual phase steels. [29].

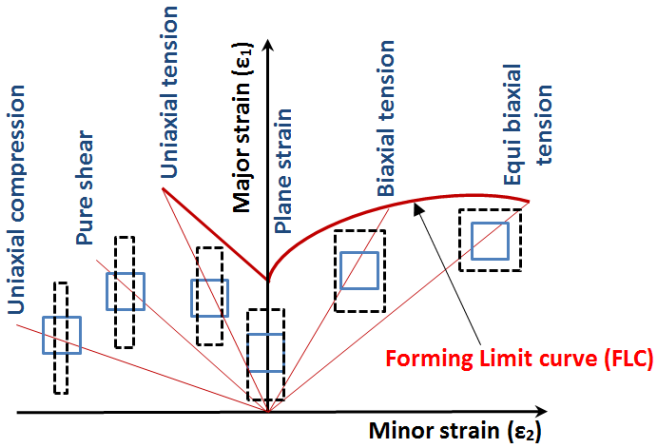


Fig. 1. Schematic representation of forming limit diagram (FLD) [26, 28, 29]

Often, the process technology varies according to the desired goal. The parameters affecting the formability of sheets are numerous and include among others: pressure, speed, thickness of the sheet, lubrication, or even the initial state of the material and the

thermal or mechanical treatment it has undergone. Furthermore, the output responses depend largely on the combination of the parameters between them and the resulting interactions. However, industrial deep drawing operations are based on the constancy of working conditions and parameters. Thus, in a technical-economic concern, the present work aims to study by experimental approach the influence of the blank holder pressure on the damages of the deep drawn parts of DD14 steel sheets and by numerical simulation the forming operation speed and the BHP amplitude on the material plastic instability, using an explicit finite element model from Abaqus/CAE software. The aim is to identify the optimum levels of process parameters that minimize the risk of necking and fracture during plastic instability of deep-drawn metal sheets. The anisotropy of the material was demonstrated from uniaxial traction tests carried out on specimens taken in three different directions. The FLC plots served as a fundamental tool for formability optimization. Finally, the practical execution and simulation of the deep drawing test made it possible to locate areas with high plastic instability.

## 2. Experimental Method

### 2.1. Material

The material studied is a mild steel grade DD14 complying with European standard EN 10111. The choice of this material is motivated by its large-scale use in the company's workshop GEMELEC El Kouif Tebessa, Algeria. The chemical composition mainly consists of 0.08%C, 0.35%Mn and 0.03%Si. The material is delivered in the hot-rolled, pickled and oiled state and has the mechanical properties given in Table 1.

Table 1. Tensile properties of DD14 steel

| EN 10111 | Mechanical characteristics | | |
|---|---|---|---|
| | Re | Rm | A90 |
| DD14 | (MPa) | (MPa) | % |
| | 220-280 | 320-370 | ≥ 33 |

The microstructure was revealed by surface chemical attack with Nital-based reagent, on previously coated and polished samples. Metallographic observation is made by a Nikon Eclipse LV100ND Microscope, with a magnification of 100x. revealed a ferritic microstructure hardened on the surface with different sizes of grains more or less elongated in the rolling direction (RD) likewise certain carbides (C) and sulfide inclusions (S) appeared at the grain boundaries (Fig. 2).

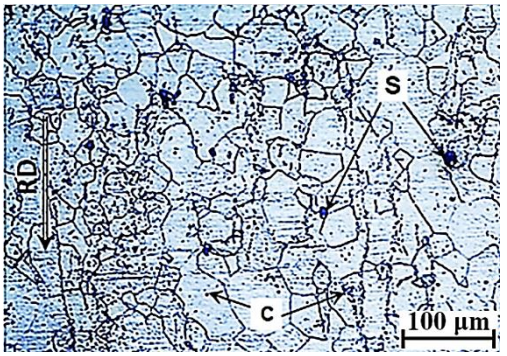


Fig. 2. Optical micrography of Microstructure of DD14 steel sample

### 2.2. Tensile Test

In order to highlight the material's anisotropy and its influence on mechanical behavior, uniaxial tensile tests were carried out on specimens taken in three directions (0°, 45° and 90°) with respect to the sheet's rolling direction (Fig. 3-a). The tests are carried out according to standard NF EN 10002-1 on a Zwick/Roell Z050 uniaxial tensile machine at room temperature, with a speed of 100 mm/min. Fig. 3-b shows the specimen geometry.

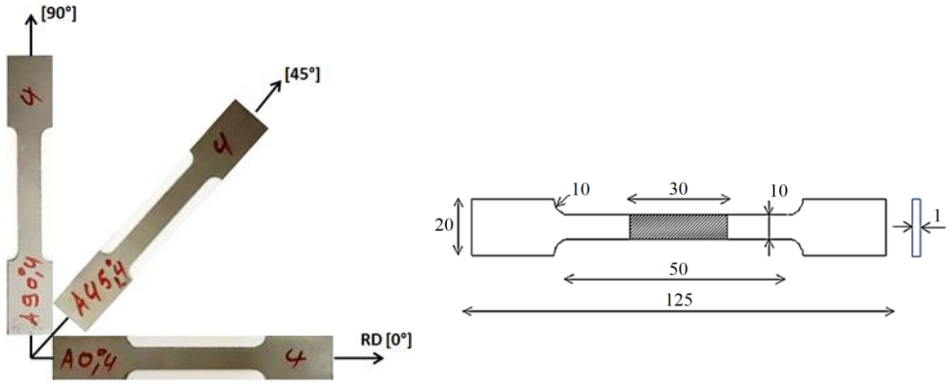


a) b)

Fig. 3. Uniaxial tensile test specimen NF EN 10002, Sampling and geometry

Furthermore, the material's consolidation is supposed to obey Holloman's hardening law Eq (1) [30]. Thus, the hardening exponent (n) and the strength coefficient (K) of this law were estimated from the rational tensile curves.

$$\sigma_v = K\varepsilon_r{}^n \tag{1}$$

Where: $\varepsilon_r$ and $\sigma_v$ are true strain and true stress respectively.

### 2.3. Deep Drawing Test

The test was conducted industrially. Before submitting to the metal forming, a grid was drawn on the blank to be deep-drawn allowing the major and minor strains to be measured, to visualize their paths and to locate the most subjected areas to plastic strain for each test. In order to avoid unnecessary superposition and cluttering of experimental points on the FLC curve, squares of dimensions 50x50 mm² were chosen according to blank size and deep-drawn part geometry (Fig. 4).

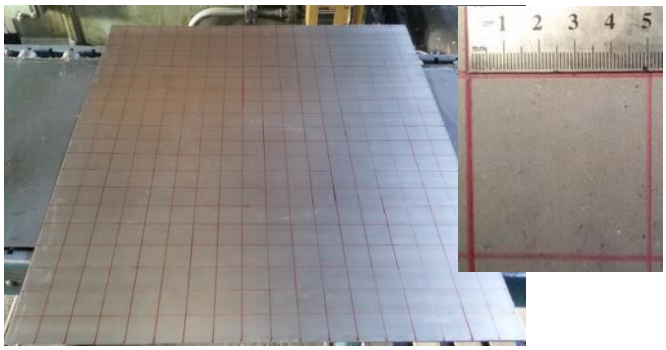


Fig. 4. Grid drawn on the blank

The tests were conducted with two main parameters, namely: die pressure (DP) and blank holder pressure (BHP). The forming action is obtained from the simultaneous displacement of the die and the blank holder, between them is held the blank, towards fixed punch on the press table. However, the blank holder pressure is the variable parameter in the tests.

### 2.4. Modelling and Numerical Simulation

The material studied is characterized by anisotropic elastoplastic behavior. Anisotropy was taken into account in the numerical simulation through the Hill48 criterion [31]. This criterion states that the classical elastic function is the most important and frequently used method for metallic materials plastic anisotropy détermination. A rectangular Cartesian stress component can be used to express this extension of the isotropic Von Mises function, as follows Eq (2) [32]:

$$2f = F(\sigma_{yy} - \sigma_{zz})^2 + G(\sigma_{zz} - \sigma_{xx})^2 + H(\sigma_{xx} - \sigma_{yy})^2 + 2L{\sigma_{yz}}^2 + 2M{\sigma_{zx}}^2 + 2N{\sigma_{xy}}^2 = 1 \quad (2)$$

Where F, G, H, L, M and N are the Hill anisotropy coefficients, which can be expressed as follows Eq (3) [33]:

$$F = \frac{1}{2}\left(\frac{1}{R_{22}^2} + \frac{1}{R_{33}^2} - \frac{1}{R_{11}^2}\right)$$
$$G = \frac{1}{2}\left(\frac{1}{R_{11}^2} + \frac{1}{R_{33}^2} - \frac{1}{R_{22}^2}\right)$$
$$H = \frac{1}{2}\left(\frac{1}{R_{11}^2} + \frac{1}{R_{22}^2} - \frac{1}{R_{33}^2}\right) \quad (3)$$
$$L = \frac{3}{2R_{23}^2}$$
$$M = \frac{3}{2R_{13}^2}$$
$$N = \frac{3}{2R_{12}^2}$$

Where R11, R22, R33 and R12 are the Hill anisotropy ratios that specify the material in the Abaqus FEM software.

These parameters can be expressed as follows in Eq (4) [33-34]:

$$R_{11} = R_{13} = R_{23} = 1$$
$$R_{22} = \sqrt{\frac{r_{90}(r_0+1)}{r_0(r_{90}+1)}}$$
$$R_{33} = \sqrt{\frac{r_{90}(r_0+1)}{(r_{90}+r_0)}} \quad (4)$$
$$R_{12} = \sqrt{\frac{3r_{90}(r_0+1)}{(2r_{45}+1)(r_{90}+r_0)}}$$

In the thin sheet metal forming process, the plane stress state is generally predominant. Consequently, only the four coefficients: F, G, H and N can be retained. These factors can be determined empirically from a monotonic tensile test following various sampling directions Eq (5) [35].

$$F = \frac{r_0}{r_{90}(1+r_0)}$$
$$G = \frac{1}{1+r_0}$$
$$H = \frac{r_0}{1+r_0} \quad (5)$$
$$N = \frac{(r_0+r_{90})(2r_{45}+1)}{2r_{90}(1+r_0)}$$

Where $r_0$, $r_{45}$ and $r_{90}$ are the values of the anisotropy coefficient (r) according to the directions, 0°, 45° and 90° with respect to the rolling direction respectively.

The anisotropy coefficient (r) is defined by the ratio of transverse strains Eq (6) [36]:

$$r = \frac{\varepsilon_2}{\varepsilon_3} = \frac{ln\frac{b}{b_0}}{ln\frac{t}{t_0}} \quad (6)$$

Where $\varepsilon_2$ and $\varepsilon_3$ are the strains in the width ($b_0$) and thickness ($t_0$) directions, respectively.

The stamping operation was simulated as performed industrially in the GEMELEC unit workshop. All experimental conditions were respected. The numerical deep drawing simulation model is run in 3D using Abaqus/CAE software. Fig. 5 shows the configuration of the forming tools and the blank. The geometry and mesh of the model are presented in the longitudinal section plane.

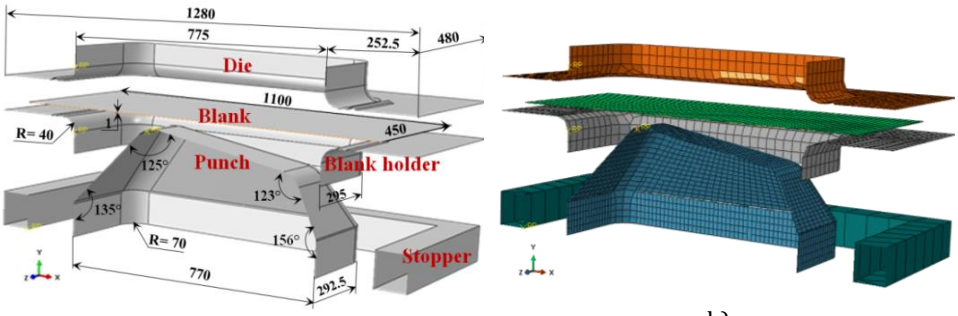


a) b)

Fig. 5. Forming tools and blank, a) Drawing and b) Meshing

The boundary conditions for the simulation model have been derived from the different operations of the deep drawing manufacturing range (Fig. 6). The forming action is obtained by the die and the blank holder moving where between which the blank is maintained, compared to the fixed punch on the machine table. The die action takes place under controlled pressure until it reaches its final position once displaced 25mm.

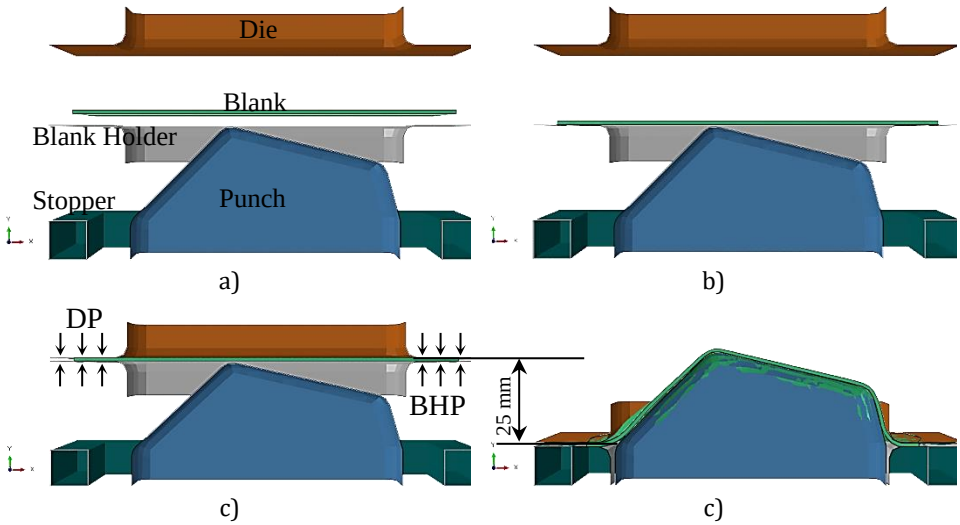


Fig. 6. Deep drawing manufacturing range; a) Initial position, b) Blank set-up, c) Die action and application of BHP and d) Final position after 25 mm stroke

## 3. Results and Discussion

### 3.2. Tensile Test

Fig. 7 shows the true stress-true strain curve for the uniaxial tensile test. The sampling direction does not affect the material's behavior, as the curves show the same trends in both elastic and plastic deformation domains with presence of the Piobet-Lüders phenomenon. The slopes of the linear part of the three specimens seem to be confused, although Table 2 shows that tensile properties are weakest in the rolling direction and stiffness in terms of Young's modulus is highest when the material is tested in the 45° direction.

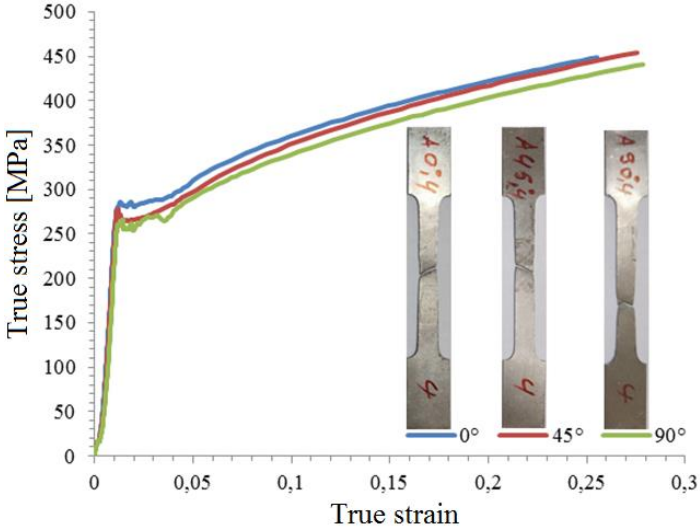


Fig. 7. Influence of sampling direction on true stress-true strain curves

This seems to be due to the material's low anisotropy ($r_{45}$=0.8) in this direction. Rolling the sheet did not change the material's ability to undergo strain-hardening, whose coefficient (n=0.24) remained constant regardless of the direction in which the specimen was taken, Table 2.

However, for all three samples tested, the curves show a discontinuity of Re, which explains the material's sensitivity to the Piobet-Lüders phenomenon and consequently the appearance of two elastic limits ($Re_H$ and $Re_L$). The rolling direction is the most advantageous for this property and even offers the best tensile strength (Rm) without sensitively affecting the material's elongation at fracture (Agt(corr). = 0.31%). The transverse direction (90°) is the least favorable for all tensile properties. The curve relating to this sampling direction shows the widest elastoplastic transition range and a more marked instability phenomenon (Necking) on the tensile specimen.

Table 2. Mechanical properties of DD14 steel

| Direction | E (GPa) | $Re_H$ (MPa) | $Re_L$ (MPa) | Rm (MPa) | Agt(corr.) % | r | n | K (MPa) |
|---|---|---|---|---|---|---|---|---|
| 0° | 136,83 | 281,56 | 275,13 | 347,83 | 0.31 | 1,10 | 0.24 | 622,28 |
| 45° | 148,88 | 275,35 | 260,36 | 344,99 | 0.32 | 0,83 | 0.24 | 620.17 |
| 90° | 126,23 | 257,79 | 248,50 | 333,67 | 0.32 | 1,11 | 0.24 | 594.48 |

### 3.2. Deep Drawing Test

*3.2.1 Influence of Blank Holder Pressure*

The evaluation of deformations was done by optical tracking. The observation made it possible to locate areas of necking or fractures, as well as the path of major and minor strains of each grid square. The measured values make it possible to plot the material's forming limit curve (FLC) (see section 3.2.2).

Fig. 8 shows an example of the deformation of the most solicited squares, in this case, the bottom front corners of the deep drawn part. The orientation of the grid lines enables us to determine the strain path and locate areas at risk of plastic instability. Under the deep drawing conditions shown in Fig. 8-a, the deformation path of the grid is indicated by the arrows oriented towards the front corners of the deep drawn part where the fracture is likely to occur.

These observations confirm those of Ref. [37], which show that due to excess material and/or a large difference between the corners, fractures initiate in the lower corners of the rectangular deep drawn part and then propagate diagonally.

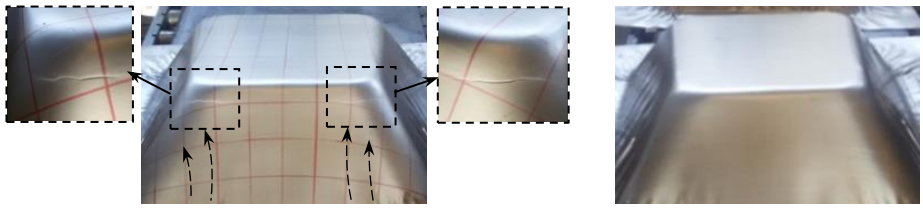

a) b)

Fig. 8. Morphology of deep drawn parts under conditions; a) DP = 14 MPa, BHP = 10 MPa and b) DP = 14 MPa, BHP = 7 MPa

The extent of damage can be reduced or even spared if the deep drawing conditions are mastered. Figure 8-b shows that reducing the blank holder pressure gives a deep drawn part without necking and without fracture. However, this low pressure causes a slight increase in the wrinkle size which can affect the choice of the finished product quality.

Nevertheless, the phenomenon of wrinkling is not considered a reason for product rejection for the company. It is still necessary to optimize the deep drawing parameters to successfully complete the operation with the best quality.

*3.2.2 Forming Limit Curve (FLC)*

The FLC is a key result for judging sheet metal formability, both experimentally and in numerical simulation of the deep drawing process. The technique for plotting the FLC curve is inspired by Hecker's method of determining the limiting deformations; the simplicity of this method has led to its widespread use [38]. Therefore, for reasons of reducing the measures, only the most stressed squares and where the fracture could take place are taken into account (Fig. 9). For each numbered square, it is possible to locate and measure the deformations [39-41].

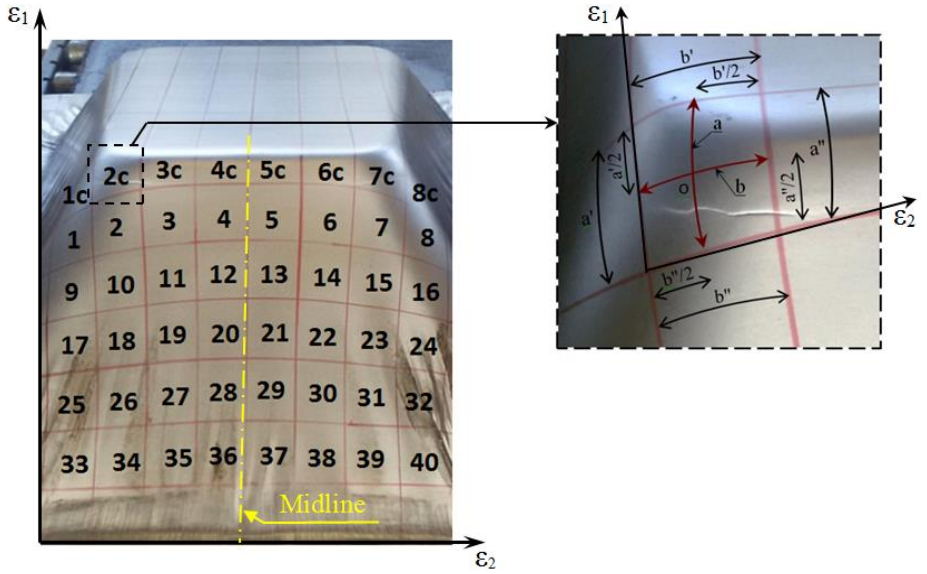


Fig. 9. Measuring method of grid deformations

For better precision and to minimize random measurement errors, the dimensions of the deformed squares are evaluated relatively. To do this, the four sides (a', a", b', b") of the deformed square are measured individually. The final dimensions (a and b) to be retained are measured between the centers of opposite sides two by two. The major and minor engineering strains are calculated as follows Eqs. (7)-(8) for evaluating the true major and true minor strains by Eq (9) [28].

$$e_1 = \frac{a-a_0}{a_0} \tag{7}$$

$$e_2 = \frac{b-b_0}{b_0} \tag{8}$$

$$\varepsilon_{1,2} = ln\,(1 + e_{1,2}) \tag{9}$$

The graphic representation of the true strains in a reference frame ($\varepsilon_1$,$\varepsilon_2$) makes it possible to trace the FLC (Fig. 10).

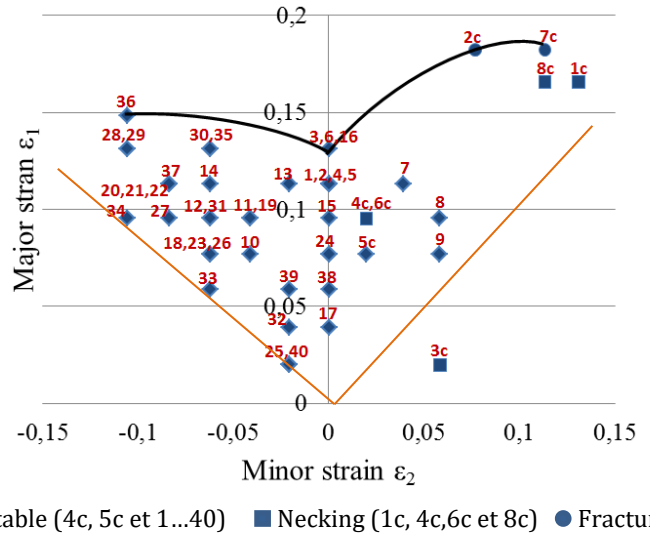


Fig. 10. Experimental strains distribution during deep drawing of DD14 steel

It emerges from the analysis of this FLC curve that the limit points of strains (36, 3, 16, 2c and 7c) are those of the squares located at the deep drawn part bottom corners (2c and 7c) or at the edge of that (36, 16). In return, the majority of the squares were located in the uniaxial traction zone and some of them (25, 40, 32 and 33) located in the deep drawn part wall were deformed in the wrinkle form. Some grid elements traced on the sheet have undergone biaxial expansion (4c, 5c, 6c, 7, 8, 9) or insufficient traction (3c). The squares measured at the corners (1c, 2c, 7c and 8c) having suffered the fracture, are closest to the deep drawn part bottom where the sheet metal is more solicited to the balanced expansion, caused by the punch corner.

Some experimental points on the FLC curve were superimposed, which translates to the existence of deformation symmetry in areas equidistant from a midline between the frontal corners of the deep drawn part (Figure 8). The pairs of squares having undergone the same deformation during forming operation are located either on the front wall of the deep drawn part (3-6), (4-5), (18-23), (20-21) and (28-29) or on the corner of the latter, like pairs (1c-8c) and (2c-7c), with the exception of their minor strains which create a slight lack of symmetry. Generally, it was found that symmetry affects only 29.16% of the formed area, suggesting unstable elastoplastic behavior of the material during the deep drawing and that the tooling of the operation needs fine-tuning.

*3.2.3 Modeling and Numerical Simulation*

The anisotropy parameters (F, G, H, N) of the Hill 48 criterion and the anisotropy ratios (R11, R22, R33, R12, R13 and R23) are calculated from Eqs. (3)-(4). The obtained values in Table 3 are directly injected into the finite element calculation code Abaqus/CAE for numerical simulation of the deep drawing process.

Table 3. Anisotropic parameters for DD14 steel

| Hill48 anisotropy coefficients | | | | Anisotropy ratios | | | |
|---|---|---|---|---|---|---|---|
| F | G | H | N | R11\|R13\|R23 | R22 | R33 | R12 |
| 0,468 | 0,475 | 0,524 | 1,260 | 1 | 1,003 | 1,029 | 1,091 |

A numerical simulation carried out under lubrication conditions with a coefficient of friction f=0.05 and pressures DP= 14 MPa, BHP= 10 MPa provided a result almost identical to that of the experimental procedure (Fig. 11). Indeed, it can be seen that the major strain of the most solicited area is located at the front corners of the deep drawn part bottom.

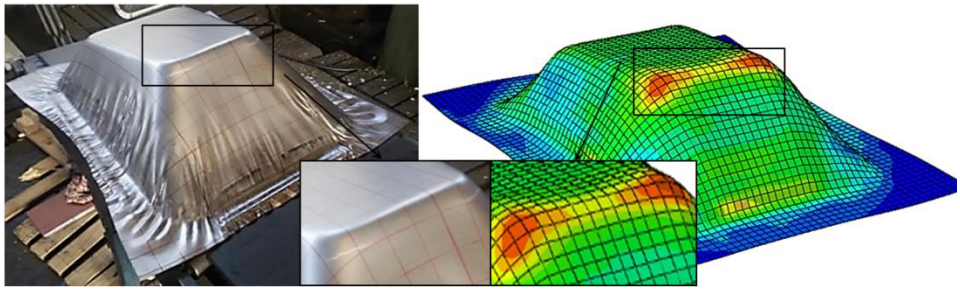

a) b)

Fig. 11. Representation of deep-drawn, a) Experimental, b) Numerical simulation

For a deeper comparative analysis, the selected nodes for strain measurement were chosen in the same way as the experimental procedure (Fig. 12). The results of major and minor plastic strains measured at each node by the finite element code Abaqus/ CAE (PE22, PE11), allowed us to determine the true FLC curve according to Eq (9). Where PE11 is plastic strain component following the x-axis and PE22 is plastic strain component following the y-axis.

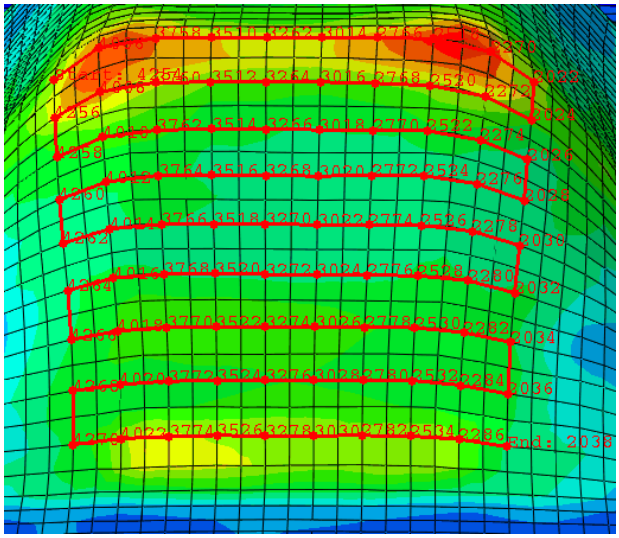

Fig. 12. Path of nodes concerned by the analysis

To adapt the operation time to the amplitude of the forming load, the simulation of the deep drawing operation was carried out by combining the "Step" module with "Load-Amplitude" in the finite element calculation code Abaqus/CAE. The numerical simulation took place in several scenarios, playing on the amplitude of the forming load and the execution time of the deep drawing operation. The best scenario results from a simulation conducted with DP=14 MPa and BHP=10 MPa (Fig. 13).

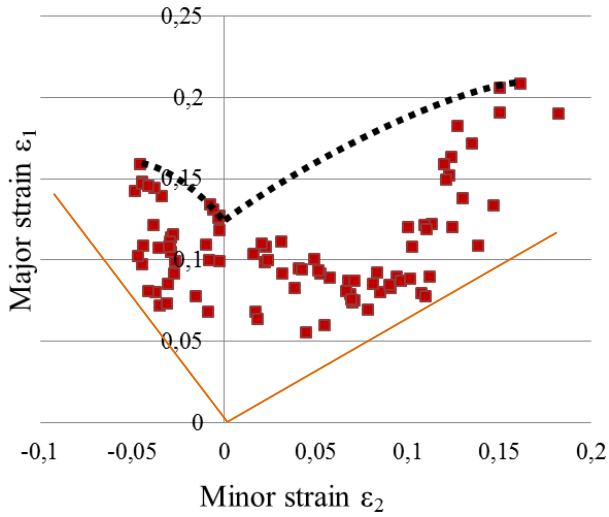


Fig. 13. Numerical simulation strains distribution during deep drawing of DD14 steel

Considering the maximum points for each deformation mode of the simulation FLC, respectively the uniaxial, planar and equi-biaxial modes, allowed us to determine the experimental-simulation comparative FLC curve.

The optimal FLC thus deduced shows the same trend as that obtained from the experimental test, though the material's formability range has expanded by 2% and 5% in terms of major and minor strains simultaneously (Fig. 14).

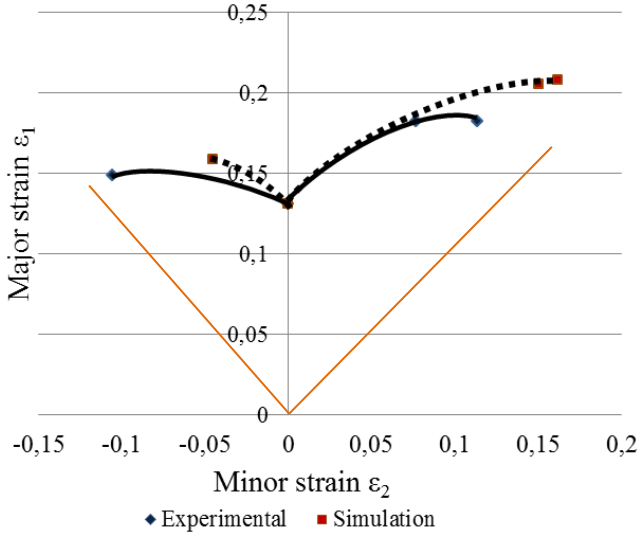


Fig. 14. Forming limit curve of DD14 steel

However, it should be noted that an adequate correlation between the amplitude of the forming load and the operation time enables the sheet to better adapt to equi-biaxial strain modes, according to the final geometry of the deep drawn part. These two factors are essential for optimizing formability. Numerical simulation, for its part, has shown that longer forming operation time can lead to uniform strain distribution in the sheet metal as a function of the applied load.

Comparatively with other results obtained in other similar studies, the punch corner or radius has a great influence on the damage of the deep drawn square parts. Where Fuh-Kuo et al. [42] studied the effect of punch radius in square-deep drawn parts. According to the findings, a larger punch radius enables a uniform material flow under the punch profile at corners, which delays the occurrence of fractures. Ravindra et al. [43] Confirmed, the punch-die corner region of a square cup has a smoother flow of material with an increase in the punch or die profile radius. As a result, the maximum width of the flange earring is decreased. Bouchaâla et al. [44] concluded that in the deep drawing process, the die shoulder radius and punch nose radius play a major role in force distribution and material flow during the forming operation, and so on...

## 4. Conclusions

Plastic instability is manifested by a localization of plastic strain and is characterized by a weakening of the specimen section, leading to the fracture during the material forming. This study aims to better localize the phenomenon of plastic instability and reduce its undesirable effect during the deep drawing of DD14 steel sheets for a given geometry of deep-drawn parts. The following conclusions can be brought.

- The uniaxial tensile test provided a curve characterized by a discontinuity at the elastoplastic transition (Re), confirming the material's sensitivity to the Piobert-Lüders phenomenon. This phenomenon is more pronounced on specimens taken in the transverse direction (90°) compared to that of rolling.
- Hecker's method, more than being simple, allows us to accurately translate each strain measurement of grid squares into a well-identified experimental point in the FLC curve.
- The CLF of the material in the studied area shows the strain distribution, such that in the majority of cases, the strain cloud is in uniaxial and plane traction. Particularly, the located points in equi-biaxial deformation mode in the curve are the measured squares at the corners of the deep drawn part.
- The areas at a major risk of plastic instability were identified at the front corners of the deep drawn part bottom. Forming with low blank holder pressure leads to the appearance of wrinkles and makes it difficult for the material to flow. In return, high pressure causes fracture which begins in the sharp corners at the deep drawn part bottom where the diffuse necking is located at the end of the operation.
- Numerical simulation provided an FLC in good agreement with that deduced from the experimental test, through which the formability was optimized.
- Numerical simulation under various scenarios involving anisotropy, operation time and forming load amplitude has enabled us to predict the deformation modes experienced by the sheet to be deep drawn, risk areas to fracture and consequently to get a deep drawing optimal model.

This study could be extended to take into account all these factors, such as mechanical material behavior, punch corner radius, punch-die clearance, tool surface finish, friction and non-uniform blank thickness distribution, through a complete experimental test design to better surround the problem of plastic instability and make the deep drawing operation more successful.

## Nomenclature

- $A_{gt(corr)}$. Total elongation for higher traction force
- $A_{90}$ Elongation at break in 90° direction (%)
- K Strength coefficient
- n Hardening coefficient
- r Anisotropy coefficient
- Re Yield strength (MPa)
- $Re_H$ Upper yield strength (MPa)
- $Re_L$ Lower yield strength (MPa)
- Rm Tensile strength (MPa)
- BHP Blank holder pressure (MPa)
- DP Die pressure (MPa)
- $\sigma_v$ True stress (MPa)
- $\varepsilon_r$ True strain (%)
- $\varepsilon_1$ Major strain (%)
- $\varepsilon_2$ Minor strain (%)
- PE11 Plastic strain component following x-axis
- PE22 Plastic strain component following y-axis

## Abbreviations

- FLC Forming Limit Curve
- FEM Finite Element Method
- BHP Blank Holder Pressure
- DP Die Pressure

## Acknowledgment

We would like to thank the companies Sarl GEMELEC El Kouif- Tebessa, Anabib-tgt El malabiod- Tébessa and the metallurgy department of Badji Mokhtar University- Annaba (Algeria) for providing us with all the means available to succeed in this study.

## References

[1] Hollomon JH. Tensile deformation. Aime Trans, 1945; 12: 1 - 22.
[2] Cottrell AH, Bilby BA. Dislocation theory of yielding and strain ageing of iron. Proceedings of the Physical Society. Section A, 1949; 62 - 49.
[3] Ebenberger P, Uggowitzer PJ, Kirnstötter S, Gerold B, Zaefferer S, Pogatscher S. Processing-controlled suppression of Lüders elongation in AlMgMn alloys. Scripta Materialia, 2019; 166: 64 - 67. https://doi.org/10.1016/j.scriptamat.2019.02.047
[4] Hu H. Effect of solutes on lüders strain in low-carbon sheet steels. Metallurgical Transactions A, 1983; 14: 85 - 91. https://doi.org/10.1007/BF02643741
[5] Mazière M, Luis C, Marais A, Forest S, Gaspérini M. Experimental and numerical analysis of the Lüders phenomenon in simple shear. International Journal of Solids and Structures, 2017; 106: 305 - 314. https://doi.org/10.1016/j.ijsolstr.2016.07.026
[6] Wenman MR, Chard-Tuckey PR. Modelling and experimental characterization of the Lüders strain in complex loaded ferritic steel compact tension specimens. International Journal of Plasticity, 2010; 26: 1013 - 1028. https://doi.org/10.1016/j.ijplas.2009.12.005
[7] Mao B, Liao Y. Modeling of lüders elongation and work hardening behaviors of ferrite-pearlite dual phase steels under tension. Mechanics of Materials, 2019; 129: 222 - 229. https://doi.org/10.1016/j.mechmat.2018.11.015

[8] Tsukahara H, Iung T. Finite element simulation of the Piobert–Lüders behavior in an uniaxial tensile test. Materials Science and Engineering: A, 1998; 248: 304 - 308. https://doi.org/10.1016/S0921-5093(97)00857-5
[9] Sun HB, Yoshida F, Ma X, Kamei T, Ohmori M. Finite element simulation on the propagation of Lüders band and effect of stress concentration. Materials Letters, 2003; 57: 3206 – 3210. https://doi.org/10.1016/S0167-577X(03)00036-3
[10] Keeler SP. Forming Limit Criteria-Sheets. In Advances in deformation processing; Springer: Boston, MA, 1978; 127 - 157. https://doi.org/10.1007/978-1-4613-4024-9_4
[11] Boudeau N, Gelin JC. Necking in sheet metal forming. Influence of macroscopic and microscopic properties of materials. International Journal of Mechanical Sciences, 2000; 42: 2209 - 2232. https://doi.org/10.1016/S0020-7403(00)00003-5
[12] Doege E, El-Dsoki T. Deep-Drawing Cracks-Stretching Cracks: Two Different Types of Cracks in Deep-Drawing Processes. Journal of Materials Processing Technology, 1992; 32: 161 - 168. https://doi.org/10.1016/0924-0136(92)90173-P
[13] Jain M, Allin J, Lloyd JD. Fracture limit prediction using ductile fracture criteria for forming of an automotive aluminum sheet. International Journal of Mechanical Sciences, 1999; 41: 1273 - 1288. https://doi.org/10.1016/S0020-7403(98)00070-8
[14] Kardan M, Parvizi A, Askari A. Influence of process parameters on residual stresses in deep-drawing process with FEM and experimental evaluations. Journal of the Brazilian Society of Mechanical Sciences and Engineering, 2018; 40: 157 - 169. https://doi.org/10.1007/s40430-018-1085-9
[15] Hamza F, Boussaid O, Tadjine K. Study by Numerical Simulation of the Deep Drawing Parameters-Material during the Wheelbarrow Forming. Materials Science Forum. Trans Tech Publications Ltd, 2017; 895: 94-98. https://doi.org/10.4028/www.scientific.net/MSF.895.94
[16] Habeeb HA, Jweeg MJ, Khleif AA. Effect of the Single-Point Incremental Forming Process Parameters on the Surface Roughness of Aluminum Alloy Al 2024-O Draw Pieces. Advances in Science and Technology. Research Journal, 2023; 17: 155-163. https://doi.org/10.12913/22998624/174364
[17] Edis R, Sinmazcelik T, Erturk AT. Measuring applied force and energy consumption in deep drawing die Sets: An experimental and numerical analysis of CrN and CrTiN PVD coating effects. Measurement, 2024; 224: 113841. https://doi.org/10.1016/j.measurement.2023.113841
[18] Torkar M, Tehovnik F, Podgornik B. Failure analysis at deep drawing of low carbon steels.Engineering Failure Analysis, 2014; 40: 1 - 7. https://doi.org/10.1016/j.engfailanal.2014.02.003
[19] Ma B, Liu ZG, Jiang Z, Wu X, Diao K, Wan M. Prediction of forming limit in DP590 steel sheet forming: An extended fracture criterion. Materials & Design, 2016; 96: 401 - 408. https://doi.org/10.1016/j.matdes.2016.02.034
[20] Butuc MC, Barlat F, Gracio JJ, da Rocha AB. A new model for FLD prediction based on advanced constitutive equations. International journal of material forming, 2010; 3: 191 - 204. https://doi.org/10.1007/s12289-009-0667-6
[21] Matin PH, Smith LM, Petrusevski S. A method for stress space forming limit diagram construction for aluminum alloys. Journal of materials processing technology, 2006; 174: 258 - 265. https://doi.org/10.1016/j.jmatprotec.2006.01.008
[22] Stoughton TB, Yoon JW. Path independent forming limits in strain and stress spaces. International Journal of Solids and Structures, 2012; 49: 3616 - 3625. https://doi.org/10.1016/j.ijsolstr.2012.08.004
[23] Li H, Li G, Gao G, Zhang W, Wu X. A formability evaluation method for sheet metal forming with non-linear strain path change. International Journal of Material Forming, 2018; 11: 199 - 211. https://doi.org/10.1007/s12289-017-1342-y

[24] Kumar DR. Formability analysis of extra-deep drawing steel. Journal of Materials Processing Technology, 2002; 130: 31 - 41. https://doi.org/10.1016/S0924-0136(02)00789-6
[25] Aghaie-Khafri M, Mahmudi R. Predicting of plastic instability and forming limit diagrams. International Journal of Mechanical Sciences, 2004; 46: 1289 - 1306. https://doi.org/10.1016/j.ijmecsci.2004.08.009
[26] Paul SK. Theoretical analysis of strain- and stress-based forming limit diagrams. The Journal of Strain Analysis for Engineering Design, 2013; 48: 177 - 188. https://doi.org/10.1177/0309324712468524
[27] Paul SK. A critical review on hole expansion ratio. Materialia, 2020; 9: 100566. https://doi.org/10.1016/j.mtla.2019.100566
[28] Paul SK. Controlling factors of forming limit curve: a review. Advances in Industrial and Manufacturing Engineering, 2021; 2: 100033. https://doi.org/10.1016/j.aime.2021.100033
[29] Paul SK. Effect of forming strain on low cycle, high cycle and notch fatigue performance of automotive grade dual phase steels: A review. Forces in Mechanics, 2023; 100184. https://doi.org/10.1016/j.finmec.2023.100184
[30] Sing WM, Rao KP. Role of strain-hardening laws in the prediction of forming limit curves. Journal of Materials Processing Technology, 1997; 63: 105-110. https://doi.org/10.1016/S0924-0136(96)02608-8
[31] Rodney H. A theory of the yielding and plastic flow of anisotropic metals. Proceedings of the Royal Society of London. Series A. Mathematical and Physical Sciences, 1948; 1033: 281 - 297. https://doi.org/10.1098/rspa.1948.0045
[32] Nguyen DT, Dinh DK, Thi Nguyen HM, Banh TL, Kim YS. Formability improvement and blank shape definition for deep drawing of cylindrical cup with complex curve profile from SPCC sheets using FEM. J. Cent. South Univ, 2014; 21: 27 – 34. https://doi.org/10.1007/s11771-014-1911-x
[33] Chinara M, Paul SK, Chatterjee S, Mukherjee S. Effect of planar anisotropy on the hole expansion ratio of cold-rolled DP 590 steel. Transactions of the Indian Institute of Metals, 2022; 75: 535 – 543. https://doi.org/10.1007/s12666-021-02444-x
[34] Yan Y, Wang H, Li Q. The inverse parameter identification of Hill 48 yield criterion and its verification in press bending and roll forming process simulations. Journal of Manufacturing Processes, 2015; 20: 46-53. https://doi.org/10.1016/j.jmapro.2015.09.009
[35] Ghennai W, Boussaid O, Bendjama H, Haddag B, Nouari M. Experimental and numerical study of DC04 sheet metal behavior-plastic anisotropy identification and application to deep drawing. The International Journal of Advanced Manufacturing Technology, 2019; 100: 361 – 371. https://doi.org/10.1007/s00170-018-2700-8
[36] Banabic D (ed.). Formability of metallic materials: plastic anisotropy, formability testing, forming limits. Springer Science & Business Media, 2000. https://doi.org/10.1007/978-3-662-04013-3
[37] Tschätsch H. Metal forming Practise, translated by Koth a, 2006. https://doi.org/10.1007/3-540-33217-0
[38] Banabic D. Sheet metal forming processes: constitutive modelling and numerical simulation, Springer Science & Business Media: Berlin Heidelberg, 2010. https://doi.org/10.1007/978-3-540-88113-1
[39] Goodwin GM. Application of Strain Analysis to Sheet Metal Forming Problems in the Press Shop. Sae Transactions, 1968; 380 - 387. https://doi.org/10.4271/680093
[40] Ramos GC, Stout M, Bolmaro RE, Signorelli JW, Serenelli M, Bertinetti MA, Turner P. Study of a drawing-quality sheet steel. II: Forming-limit curves by experiments and micromechanical simulations. International journal of solids and structures, 2010; 47: 2294 - 2299. https://doi.org/10.1016/j.ijsolstr.2010.04.022

[41] Ke J, Liu Y, Zhu H, Zhang Z. Formability of sheet metal flowing through drawbead–an experimental investigation. Journal of Materials Processing Technology, 2018; 254: 283-293. https://doi.org/10.1016/j.jmatprotec.2017.11.051
[42] Chen F, Huang T, Chang C. Deep drawing of square cups with magnesium alloy AZ31 sheets. International Journal of Machine Tools and Manufacture, 2003; 43: 1553-1559. https://doi.org/10.1016/S0890-6955(03)00198-6
[43] Saxena R, Dixit P. Finite element simulation of earing defect in deep drawing. The International Journal of Advanced Manufacturing Technology, 2009; 45: 219-233. https://doi.org/10.1007/s00170-009-1963-5
[44] Bouchaâla K, Ghanameh M, Faqir M, Mada M, Essadiqi E. Numerical investigation of the effect of punch corner radius and die shoulder radius on the flange earrings for AA1050 and AA1100 aluminum alloys in cylindrical deep drawing process. Heliyon, 2021; 7: 2405-8440. https://doi.org/10.1016/j.heliyon.2021.e06662